Journal of Vibration and Control

http://jvc.sagepub.com

Pattern Formation in the Rotating Cylindrical Annulus with an Azimuthal Magnetic Field at low Prandtl Numbers

Erol Kurt, Werner Pesch and Friedrich H. Busse

Journal of Vibration and Control 2007; 13; 1321
DOI: 10.1177/1077546307077455

The online version of this article can be found at:
http://jvc.sagepub.com/cgi/content/abstract/13/9-10/1321

Published by:
SAGE
http://www.sagepublications.com

Additional services and information for *Journal of Vibration and Control* can be found at:

Email Alerts: http://jvc.sagepub.com/cgi/alerts

Subscriptions: http://jvc.sagepub.com/subscriptions

Reprints: http://www.sagepub.com/journalsReprints.nav

Permissions: http://www.sagepub.co.uk/journalsPermissions.nav

Citations http://jvc.sagepub.com/cgi/content/refs/13/9-10/1321

Downloaded from http://jvc.sagepub.com at Gazi University on November 11, 2009

Pattern Formation in the Rotating Cylindrical Annulus with an Azimuthal Magnetic Field at low Prandtl Numbers

EROL KURT
Physics Department, Faculty of Arts and Sciences, Gazi University, 06500 Teknikokullar, Ankara, Turkey (ekurt52tr@yahoo.com)

WERNER PESCH
FRIEDRICH H. BUSSE
Institute of Physics, University of Bayreuth, D-95440 Bayreuth, Germany

(Received 15 April 2006; accepted 12 July 2006)

Abstract: Patterns are theoretically formed in the frame of a hydromagnetic convection induced by radial buoyancy in an electrically conducting fluid contained by a rotating cylindrical annulus with a homogeneous magnetic field (B) in the azimuthal direction. The annulus is assumed to rotate with an angular frequency, Ω under the small gap approximation with rigid cylindrical boundaries. The onset of convection is found in the form of axial, axisymmetric or oblique rolls with a broken symmetry. The roll angle Ψ depends on the ratio between the Chandrasekhar number, $Q \sim B^2$, and the Coriolis number, $\tau \sim \Omega$. In addition to fully three-dimensional ($3D$) numerical simulations, weakly nonlinear and Galerkin analyses for roll patterns are performed for Prandtl number $P = 0.1$. At finite amplitudes, secondary instabilities are encountered in the form of longwave and shortwave.

Key words: Pattern formation, convection, cylindrical annulus, secondary instability

1. INTRODUCTION

One of the most studied examples of convection instability is the fluid layer subjected to a temperature gradient. For instance, in a horizontal fluid layer heated from below and cooled from above a striped patterns of convection rolls develop. This scenario describes the famous Rayleigh–Bénard convection (RBC), as a standard paradigm of pattern formation (Cross and Hohenberg, 1993; Busse, 1978; Bodenschatz et al., 2000).

In the present case, we consider the problem of convection induced by radial buoyancy in an electrically conducting fluid contained in a rotating (angular frequency, Ω) cylindrical annulus which is cooled at the inner surface and heated from outside. In addition, an azimuthal magnetic field (B) is applied, for instance by an electrical current through the cylinder axis. The motivation of this study has come originally from the geophysical context. In planetary and stellar applications, the configuration of rotation axis and magnetic

Journal of Vibration and Control, **13(9–10):** 1321–1330, 2007 DOI: 10.1177/1077546307077455
©2007 SAGE Publications Los Angeles, London, New Delhi, Singapore

Downloaded from http://jvc.sagepub.com at Gazi University on November 11, 2009

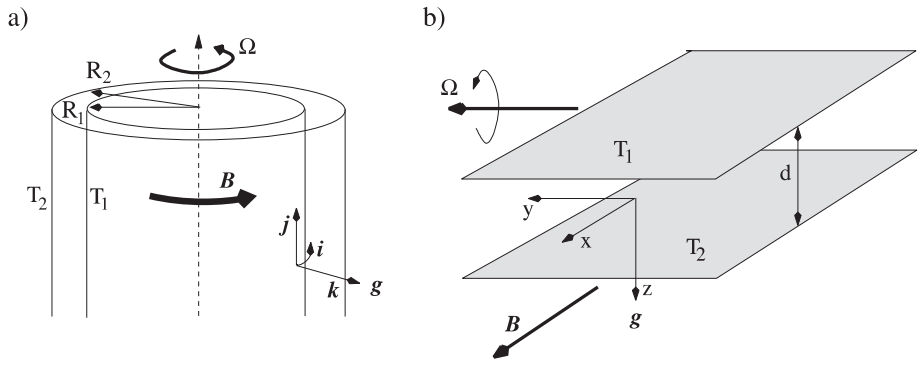

Figure 1. (a) Schematic representation of the rotating annulus. (b) The analogy to planar convection ($d \equiv R_2 - R_1$).

field direction perpendicular to each other and perpendicular to the gravity vector could be more important because it corresponds to the case of convection in the equatorial regions of rotating spherical fluid shells when an azimuthal magnetic field is imposed (Eltayeb, 1972, 1975; Busse and Finocchi, 1993; Petry et al., 1997). It is believed that the toroidal magnetic fields in the electrically conducting cores of planets or in the solar atmosphere are often much stronger than the poloidal components that can be measured from the outside. The onset of convection in this geometry was considered by Chandrasekhar (1961). He found the surprising result that Lorentz force and Coriolis force may counter each other such that the critical Rayleigh number (R_c) for the onset of convection is lower than in cases when either the magnetic field or the rotation rate vanishes. The problem is also of considerable interest from a more general point of view in that it is concerned with formations of patterns in the presence of two competing directional effects, in this case rotation and the magnetic field.

In the rotating annulus configuration (see Figure 1a), the centrifugal force is used as effective gravity and the radial direction thus corresponds to "vertical". As will be demonstrated later, a large variety of convection patterns is found at different values of Coriolis τ and Chandrasekhar Q numbers for moderate values of the Rayleigh number R.

The mathematical formulation of the problem as well as the numerical methods are discussed in Section 2. In the small gap approximation, the problem reduces to the case of a horizontal fluid layer, which is heated from below. In addition, a magnetic field, which is perpendicular to the rotation axis of the layer is considered. A Cartesian system of coordinates can be used in order to simplify the problem. A sketch of the geometrical configuration to be considered in this paper is shown in Figure 1b.

The results of the linear theory for the onset of convection, which was first considered by Eltayeb (1972) more than 30 years ago are discussed in Section 3. In order to obtain simple expressions, Eltayeb used idealized boundary conditions, namely stress-free conditions for the velocity field and electrically infinitely conducting boundaries for the magnetic field. In the present paper the more realistic case of rigid, electrically insulating boundaries is considered. Some detailed results on the dominant instabilities as well as patterns that are introduced by secondary bifurcations are given in Section 4 in the case of low Prandtl number P. The paper closes with an outlook on the results in the concluding section.

Downloaded from http://jvc.sagepub.com at Gazi University on November 11, 2009

2. DESCRIPTION OF THE PROBLEM AND METHODS

We refer to the geometrical model shown in Figure 1(b) to describe the problem. The effective gravity is provided by the centrifugal force, $g = \Omega^2(R_1 + R_2)/2$, and its direction is given by the unit vector $\vec{k}$. The upper and lower boundaries are kept at the constant temperatures T_1 and T_2, $T_2 > T_1$, respectively. In this paper we use the thickness d of the layer as the length scale, the vertical diffusion time, $\frac{d^2}{\kappa} = t_\kappa$, as the time scale, $(T_2 - T_1)/R$ as the temperature scale, and the magnetic flux density B_0 of the imposed field as the scale of the magnetic field.

Then the basic equations of motion for the velocity field $\vec{u}$, the heat equation for the deviation Θ of the temperature from the state of pure conduction and the equation of magnetic induction in dimensionless form are as follows:

$$P^{-1}\left(\frac{\partial}{\partial t} + \vec{u}\cdot\nabla\right)\vec{u} + 2\tau\,\vec{j}\times\vec{u} = -\nabla\Pi - \vec{k}\Theta + \nabla^2\vec{u} + Q(\vec{i} + \frac{\kappa}{\lambda}\vec{b})\cdot\nabla\vec{b}, \quad (1)$$

$$\nabla\cdot\vec{u} = 0, \quad (2)$$

$$\left(\frac{\partial}{\partial t} + \vec{u}\cdot\nabla\right)\Theta = -R\vec{k}\cdot\vec{u} + \nabla^2\Theta, \quad (3)$$

$$\frac{\kappa}{\lambda}\left(\frac{\partial}{\partial t}\vec{b} + \vec{u}\cdot\nabla\vec{b} - \vec{b}\cdot\nabla\vec{u}\right) = \vec{i}\cdot\nabla\vec{u} + \nabla^2\vec{b}, \quad (4)$$

$$\nabla\cdot\vec{b} = 0, \quad (5)$$

where all gradient terms in (1) have been combined into the pressure term $\nabla\Pi$. The Rayleigh number R, the Prandtl number P, the Coriolis parameter τ and the Chandrasekhar number Q are defined by

$$R = (\alpha(T_2 - T_1)gd^3)/(\nu\kappa), \quad P = \frac{\nu}{\kappa}, \quad \tau = \Omega d^2/\nu, \quad Q = ({B_0}^2d^2)/(\varrho\mu\lambda\nu), \quad (6)$$

where α, ν, κ, μ, ϱ and λ are the coefficient of thermal expansion, the kinematic viscosity, the thermal diffusivity, the magnetic permeability, the density and the magnetic diffusivity of the fluid, respectively. The magnetic field has been represented in the form $\vec{B} = B_o(\vec{i} + \frac{\kappa}{\lambda}\vec{b})$ where $\vec{i}$ is the unit vector in the x-direction. In the following we shall focus on the case of liquid metals where $\frac{\kappa}{\lambda}$ is of the order 10^{-4} to 10^{-5}. Hence we shall adopt in this paper the limit $\kappa << \lambda$ and drop the terms on the left hand side of (4) and the term multiplied by $\frac{\kappa}{\lambda}$ in equation (1).

We use a Cartesian system of coordinates with the unit vectors $\vec{i}$, $\vec{j}$, $\vec{k}$ in the direction of the x, y, $z-$ axes as shown in Figure 1. The conditions at the boundaries are then given by

$$\vec{u} = 0, \quad \Theta = 0, \quad \nabla\times\vec{b}\cdot\vec{k} = 0 \quad \text{at} \quad z = \pm\frac{1}{2}. \quad (7)$$

Downloaded from http://jvc.sagepub.com at Gazi University on November 11, 2009

The continuity of the magnetic field $\vec{b}$ across the boundaries does not have to be taken into account explicitly in the limit $\kappa << \lambda$ as will be pointed out below. As in earlier papers (Auer et al., 1995; Busse et al., 2003; Kurt et al., Pesch, 1996) we assume periodic boundary conditions in the $x, y-$plane. The agreement between the results of those papers and the experimental observations of Jaletzky and Busse (2000) indicates that the periodic boundary conditions as well as the small gap approximation are appropriate for the rotating annulus experiment at the moderate values of τ to be considered in this paper. In order to eliminate the pressure term in (1) we introduce the general representations for the solenoidal vector fields $\vec{u}$ and $\vec{b}$, (see (2) and (5)):

$$\vec{u} = \overline{\vec{u}} + \nabla \times (\nabla \times \vec{k}v) + \nabla \times \vec{k}w \equiv \overline{\vec{u}} + \vec{\delta}v + \vec{\varepsilon}w, \tag{8}$$

$$\vec{b} = \overline{\vec{b}} + \nabla \times (\nabla \times \vec{k}h) + \nabla \times \vec{k}g \equiv \overline{\vec{b}} + \vec{\delta}h + \vec{\varepsilon}g, \tag{9}$$

where overbars in $\overline{\vec{u}}$ and $\overline{\vec{b}}$ denote the average over the $x, y-$ plane of $\vec{u}$ and $\vec{b}$. The functions v, h and w, g describing the poloidal and toroidal components of the velocity and the magnetic field, respectively are uniquely defined if the conditions $\overline{v} = \overline{h} = \overline{w} = \overline{g} = 0$ are imposed. After the application of the differential operators $\vec{\delta}$ and $\vec{\varepsilon}$ on the velocity equation (1) we arrive at the following equations for v and w

$$\nabla^4 \Delta_2 v - 2\tau \frac{\partial}{\partial y} \Delta_2 w + \Delta_2 \theta + Q\vec{i} \cdot \nabla \nabla^2 \Delta_2 h = P^{-1} \left[\frac{\partial}{\partial t} \nabla^2 \Delta_2 v + \vec{\delta} \cdot (\vec{u} \cdot \nabla)\vec{u} \right], \tag{10}$$

$$\nabla^2 \Delta_2 w + 2\tau \frac{\partial}{\partial y} \Delta_2 v + Q\vec{i} \cdot \nabla \Delta_2 g = P^{-1} \left[\frac{\partial}{\partial t} \Delta_2 w + \vec{\varepsilon} \cdot (\vec{u} \cdot \nabla)\vec{u} \right]. \tag{11}$$

In addition, an equation for the mean flow $\overline{\vec{u}}$ is obtained by averaging the velocity equation (1) over the $x - y$ plane.

$$\frac{\partial^2}{\partial z^2} \overline{\vec{u}} = \frac{1}{P} \left(\frac{\partial}{\partial t} \overline{\vec{u}} - \frac{\partial}{\partial z} \overline{\Delta_2 v \left(\nabla_2 \frac{\partial}{\partial z} v + \vec{\varepsilon} w \right)} \right). \tag{12}$$

Analogously, when applying $\vec{\delta}$ and $\vec{\varepsilon}$ on (4), we obtain in the limit $\frac{\kappa}{\lambda} \to 0$

$$\nabla^2 \Delta_2 h = -\vec{i} \cdot \nabla \Delta_2 v, \tag{13}$$

$$\nabla^2 \Delta_2 g = -\vec{i} \cdot \nabla \Delta_2 w. \tag{14}$$

The heat equation (3) can now be written in the form

$$\nabla^2 \Theta + R \Delta_2 v = (\vec{\delta}v + \vec{\varepsilon}w + \overline{\vec{u}}) \cdot \nabla \Theta + \frac{\partial}{\partial t} \Theta. \tag{15}$$

In the limit $\kappa << \lambda$, the mean distortion $\overline{\vec{b}}$ of the magnetic field does not enter the problem since it vanishes. In writing equations (10)–(15) we have introduced the *horizontal*

Downloaded from http://jvc.sagepub.com at Gazi University on November 11, 2009

gradient, $\nabla_2 \equiv \nabla - \vec{k}\vec{k} \cdot \nabla$, and the horizontal Laplacian, $\Delta_2 \equiv \nabla_2 \cdot \nabla_2$. In line with (7, 9) the basic equations (10)–(15) must be solved subject to the boundary conditions

$$v = \frac{\partial}{\partial z} v = w = \Theta = g = 0 \quad \text{at} \quad z = \pm\frac{1}{2}. \tag{16}$$

The equation (13) for h and the corresponding boundary condition can be dropped, since h can be eliminated from the problem by replacing $\nabla^2 \Delta_2 h$ in (10) with $\vec{i} \cdot \nabla \Delta_2 v$ in accordance with (13). As usual we assume the idealization of an infinitely extended fluid layer in the horizontal plane, i.e. the x, y-dependence is captured by a $2D$ Fourier series.

For the methodology, a symbolic notation for the equations (10)–(15) is used in the following

$$\mathcal{C} \frac{d}{dt} \vec{V}(\vec{x}, t) = \mathcal{L} \vec{V}(\vec{x}, t) + \vec{N}(\vec{V}(\vec{x}, t) | \vec{V}(\vec{x}, t)), \quad \mathcal{L} = \mathcal{A} + R\mathcal{B}, \tag{17}$$

where the symbolic vector $\vec{V}(\vec{x}, t) = (v, w, g, \Theta, \overline{\vec{u}})$ represents the fields in equations (10)–(15). $\vec{V}(\vec{x}, t) \equiv 0$ corresponds to the ground state. The operators $\mathcal{C}$, $\mathcal{L}$, $\mathcal{A}$ and $\mathcal{B}$ are linear differential operators while $\vec{N}$ describes the quadratic nonlinearities. Note that we have made explicit the Rayleigh number, R, in the definition $\mathcal{L} = \mathcal{A} + R\mathcal{B}$ of the linear operator $\mathcal{L}$.

To describe the solution periodic in the plane of the problem posed by (10) through (15) and the boundary conditions (16) we use the Galerkin method. The boundary conditions (16) are satisfied by expansions in suitable complete sets of functions like

$$\Theta(x, y, z, t) = \sum_{n=1}^{N} \sum_{l,m=-M}^{M} \Theta_{lmn}(t) \exp\left[i(lq_x x + mq_y y)\right] \sin n\pi \left(z + \frac{1}{2}\right). \tag{18}$$

The reality of all fields requires $v_{l,m,n} = v^*_{-l,-m,n}$, etc., where the star indicates the complex conjugate.

The sum (18) will describe the solution correctly only in the limit when the parameters N and M tend to infinity. However, truncation parameters $M = 4$ and $N = 4$ have been sufficient to achieve an accuracy of about 1% in the Galerkin approach for periodic solutions. In order to assess complex spatio-temporal solutions in a large horizontal domain and also to validate the Galerkin results, we have performed direct simulations of the basic equations (1) as well using typically the truncation parameters $M = 64$ and $N = 4$. For this purpose we have adopted a well proven code originally designed for ordinary Rayleigh–Bénard (RB) convection (Pesch, 1996). The code uses, in principle, the Galerkin representation (18) and solves the horizontal dependence with a pseudo-spectral method.

3. ONSET OF CONVECTION VIA LINEAR ANALYSIS

In principle, the onset of convection (i.e. neutral curve for instability of the ground state $\vec{V}(\vec{x}, t) \equiv 0$) can be found with the help of following ansatz:

Downloaded from http://jvc.sagepub.com at Gazi University on November 11, 2009

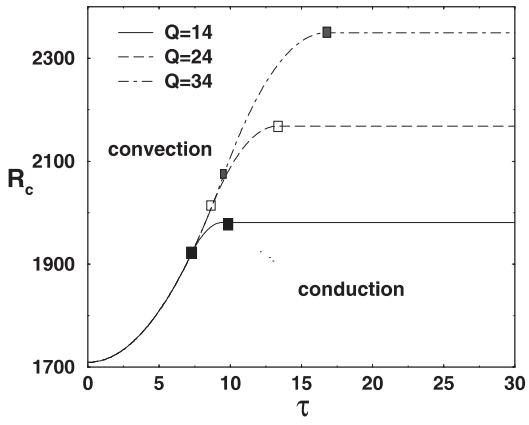

Figure 2. Critical Rayleigh numbers, R_c as a function of τ for the values $Q = 14, 24$, and 34. Oblique regions are denoted between two squares on the threshold curves for the Q values.

$$\vec{V}(\vec{x}, t) = \exp[\sigma t + i\vec{q} \cdot \vec{x}]\vec{V}_{lin}(\vec{q}, z) \tag{19}$$

in (17) which leads to the linear eigenvalue problem

$$\sigma(\vec{q}, R)\mathcal{C}\vec{V}_{lin}(\vec{q}, z) = (\mathcal{A} + R\,\mathcal{B})\vec{V}_{lin}(\vec{q}, z) \tag{20}$$

where the wavevector $\vec{q} = (q_x, q_y, 0)$ has been introduced. The condition that the maximum real part of σ vanishes, $\Re\{\sigma(\vec{q}, R)\} = 0$, determines the neutral curve, $R = R_0(\vec{q})$. The minimum of $R_0(\vec{q})$ with respect to $\vec{q}$ yields the critical wave vector $\vec{q}_c$ and the critical Rayleigh number satisfies $R_c = R_0(\vec{q}_c)$.

We have found that the onset of convection is always stationary, in other words, $\Im\{\sigma(\vec{q}, R_0)\} = 0$ holds in accordance with the findings of Eltayeb (1975) in the limit $\kappa << \lambda$. Note that the stationary threshold does not depend on the Prandtl number P. Some numerical results for R_c and $\vec{q}_c$ as function of τ are shown in Figure 2 and Figure 3(a) for some values of Q. The critical Rayleigh number, $R_c(\tau, Q)$ in Figure 2 is always equal to or larger than the Rayleigh–Bénard value $R^{RB}(\vec{q}_c) = 1708$. It increases linearly for small Q and quadratically for small τ (we refer the reader to Kurt et al., 2004 for more detailed graphs). Note also that the oblique region enlarges by Q values. According to Figure 3(a), the modulus $q_c = |\vec{q}_c|$ decreases monotonously from the RB value ($q_c = 3.116$) with increasing τ and Q. The corresponding roll angle ψ is defined as the arctan (q_{cy}/q_{cx}) and shown in Figure 3b. One observes a transition from zonal rolls ($\psi = 90^o$) to axial rolls ($\psi = 0^o$) via intermediate oblique rolls with increasing τ at fixed Q. It is also interesting that there exist "S"-shaped curves inside the oblique region (see Figure 3b).

Downloaded from http://jvc.sagepub.com at Gazi University on November 11, 2009

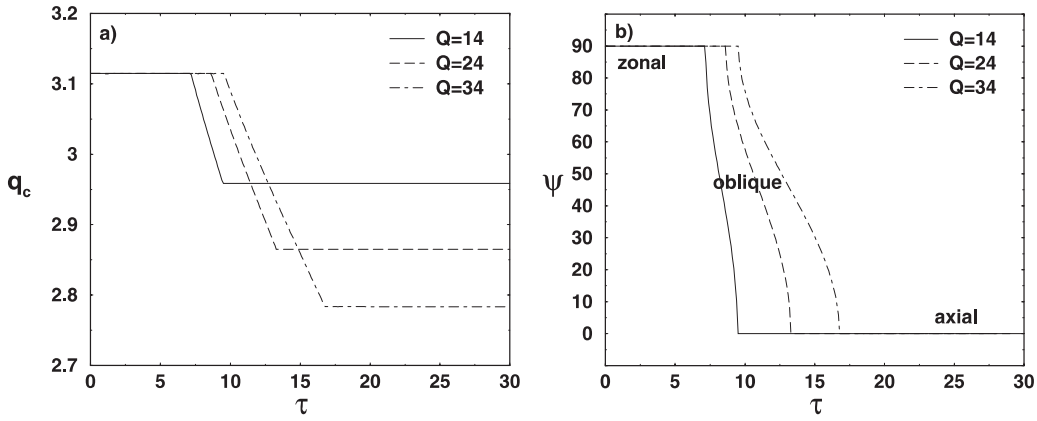

Figure 3. The corresponding wave numbers q_c (a) and the critical roll angles Ψ (b) as function of τ for $Q = 14, 24$ and 34.

4. PATTERNS AT LOW PRANDTL NUMBERS

In order to assess the nature of the primary bifurcation to rolls we first perform the standard weakly nonlinear analysis in the vicinity of $R = R_c$. We solve equation (17) with the ansatz

$$\vec{V} = A\left(\exp[i\vec{q}_c \cdot \vec{x}]\vec{V}_{lin}(\vec{q}_c, z) + c.c.\right) + V_\perp \tag{21}$$

where $c.c.$ indicates the complex conjugate and where $\vec{V}_\perp$ is of the order $\mathcal{O}(A^2)$ and orthogonal to the first term on the right hand side.

After expanding (17) in powers of A and projecting on $\vec{V}_{lin}(\vec{q}_c, z)$ one arrives at the standard amplitude equation:

$$\frac{d}{dt}A = (\epsilon_0 - \epsilon_c)A - cA^3 \tag{22}$$

with $\epsilon_o = (R - {R_c}^{RB})/{R_c}^{RB}$ and $\epsilon_c = ({R_c} - {R_c}^{RB})/{R_c}^{RB}$. Supercritical (i.e. $c > 0$) and subcritical (i.e. $c < 0$) bifurcations are found for different τ values. In a further step, the stationary nonlinear roll solutions $\vec{V}_{roll}(\vec{x})$ for a given wave vector $\vec{q}$ are determined by solving the nonlinear coupled equations (17) for the various expansion coefficients by the Newton–Raphson method. The weakly nonlinear solutions are used to provide suitable starting values for the Galerkin calculations.

The stability of rolls is examined as usual by linearizing (17) about the Galerkin solutions $\vec{V}_{roll}$ using the ansatz

$$\vec{V}(\vec{x}, t) = \vec{V}_{roll}(\vec{x}) + \exp[\sigma_n t + i\vec{s} \cdot \vec{x}]\,\delta\vec{V}(\vec{x}) \tag{23}$$

with the Floquet wave vector $\vec{s} = (s_x, s_y, 0)$. We arrive thus at a linear eigenvalue problem for $\sigma_n(R, \vec{q}, \vec{s})$. The condition $\Re\{\sigma_n\} = 0$ determines the secondary bifurcations of the rolls.

Downloaded from http://jvc.sagepub.com at Gazi University on November 11, 2009

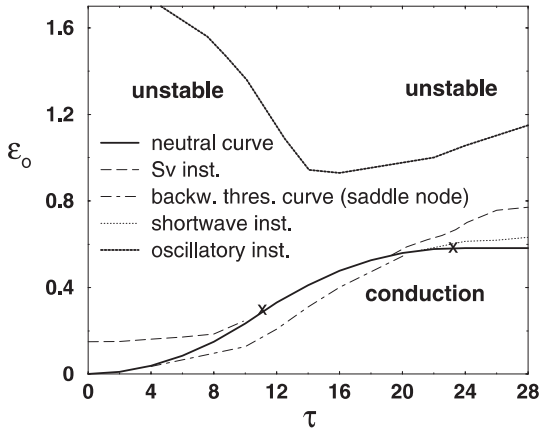

Figure 4. Stability diagram for rolls with critical wave vector $\mathbf{q}_c$ as a function of the Coriolis number τ for increasing ε_o in the case $Q = 54$, $P = 0.1$. The oblique region is between two "X" signs on the neutral curve.

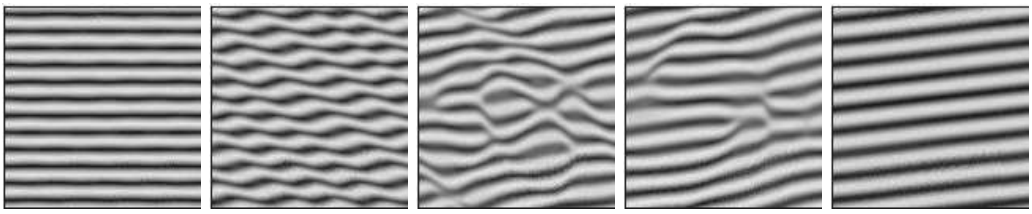

Figure 5. Transition from the zonal rolls to the oblique rolls via the Sv instability in the case $\tau = 2$, $Q = 54$, $\varepsilon_o = 0.5$ and $Pr = 0.1$. Plots from left to right correspond to times $t = 2$, 4.5, 6, 7 and 9. Aspect ratio is $\Gamma = 24$. Here and in the following figures the temperature field in the plane $z = 0.5$ is shown. The $x-$coordinate increases towards the right and the $y-$coordinate is directed upwards.

In Figure 4, a stability diagram for rolls in the case of relatively large magnetic field $Q = 54$ and $P = 0.1$ is given. At first glance, the bifurcation becomes subcritical in a fairly large τ interval ($4 \leq \tau \leq 21$). The dash-dotted line just below the neutral curve denotes the saddle-node points. Near the onset, the instabilities are found to be longwave (i.e. Sv skewed-varicose instability) at small Coriolis numbers τ. This instability mainly affects the entire region of the left side of the $\tau - \epsilon_o$ diagram. The oblique rolls are found to be stable just above the onset for moderate values of τ. At high rotation rates τ shortwave instabilities play a significant role for small ϵ_o. A detailed investigation indicates that knot instability dominates the dynamics in this parameter range. With increasing ϵ_o, oscillatory instability appears. Note also that the zonal rolls are subcritically unstable for $\tau > 15$ and this affects the dynamics at large rotation rates, qualitatively.

A typical form of the Sv instability is presented in Figure 5. Strong Sv undulations of the zonal roll pattern develop from the superimposed noise. Then the oblique rolls which has a roll angle $\Psi = 83^o$ is formed from a zonal roll. From the Galerkin analysis, we found

Downloaded from http://jvc.sagepub.com at Gazi University on November 11, 2009

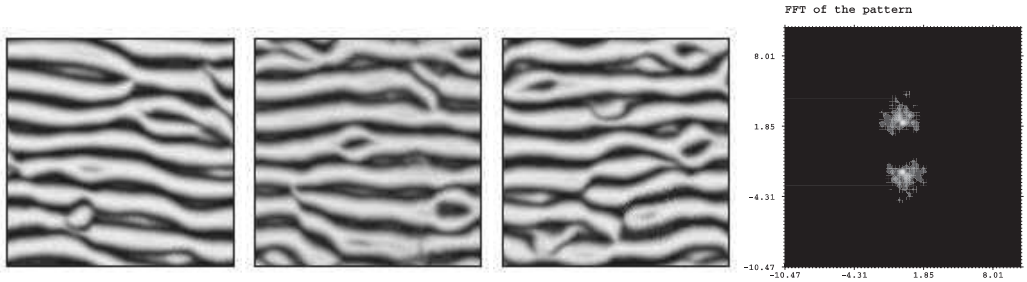

Figure 6. Patterns of chaotic zonal roll for $\tau = 8$, $Q = 54$, $\varepsilon_o = 1.3$ and $Pr = 0.1$. Random initial conditions were applied. Fourier spectrum of the last picture is shown on the right. Plots from left to right correspond to times $t = 3.75$, 5 and 6.25. Aspect ratio is $\Gamma = 20$.

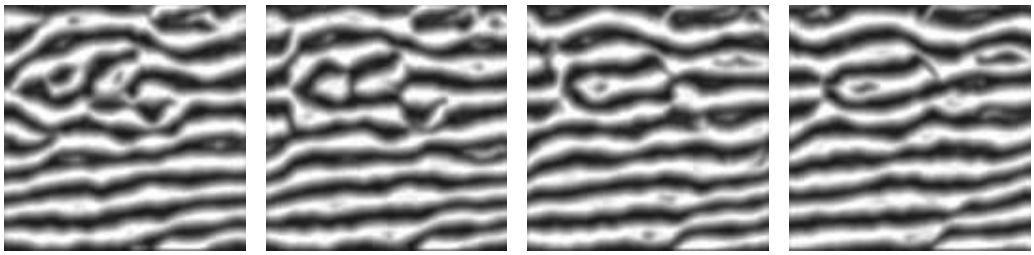

Figure 7. Oscillatory chaotic rolls at $\tau = 16$, $\epsilon_o = 1.2$, $Q = 54$. The plots from left to right correspond to the times $t = 5$, 6.5, 7 and 8.3. The aspect ratio is $\Gamma = 20$.

that the final oblique state is indeed stable above $\varepsilon_o = 0.48$. The destabilizing angle of the Floquet vector $\vec{s}$ is found to be 55^o.

In Figure 6, the patterns of typical spatio-temporal chaotic zonal roll, which occur especially for slightly larger values of τ start from random initial conditions. A Fourier spectrum of the last pattern shows that the main wave vector is along the y axis.

Oscillatory chaotic patterns are shown in Figure 7. The rolls propagate from right to left by increasing time. Spatio-temporal chaotic behaviour is also obvious due to random fluctuations in space and time.

5. CONCLUSIONS

Although only a small part of the parameter space of convection in a rotating cylindrical annulus has yet been investigated, it is obvious from the results of this paper that a large variety of patterns can be found in this problem. According to linear analysis, which determines the onset of convection, three different main periodic roll structures have been found: zonal, axial and oblique rolls. The critical Rayleigh number R_c increases with increasing τ and Q, whereas the critical wave number q_c decreases as a result of competition between rotation

Downloaded from http://jvc.sagepub.com at Gazi University on November 11, 2009

and magnetic field. The change in the roll angle from $\Psi = 90^o$ (zonal) to $\Psi = 0^o$ (axial) under increasing Coriolis number τ was found to be a smooth function of τ.

At low Prandtl numbers, the secondary instability analysis as well as time-dependent patterns showed that the general structure found in the linear analysis changes for small ε_o values. At low rotation rates, $\mathbf{\Omega}$ longwave instabilities (i.e. skewed-varicose) dominate the system. For sufficiently large ε_o values, we have mainly observed shortwave instabilities (i.e. knot) at high τ values. Spatio-temporal chaotic and oscillating patterns are widely observed at sufficiently high ε_o from simulations.

Acknowledgements. The authors gratefully acknowledge the support from the European Graduate College, under Grant No: GRK 698/1-3.

NOTE

1. On leave from Institute of Physics, University of Bayreuth, 65440 Bayreuth, Germany

REFERENCES

Auer, M., Busse, F. H., and Clever, R. M., 1995, "Three-dimensional convection driven by centrifugal buoyancy," *Journal of Fluid Mechanics* **301**, 371–382.

Bodenschatz, E., Pesch, W., and Ahlers, G., 2000, "Recent developments in Rayleigh–Bénard convection," *Annual Revues Fluid Mechanics* **32**, 709–778.

Busse, F. H., 1978, "Nonlinear properties of thermal convection," *Reports on Progress in Physics* **41**, 1929–1967.

Busse, F. H. and Finocchi, F., 1993, "The onset of thermal convection in a rotating cylindrical annulus in the presence of a magnetic field," *Physics of the Earth and Planetary Interiors* **80**, 13–23.

Busse, F. H., Zaks, M. A., and Brausch, O., 2003, "Centrifugally driven thermal convection at high Prandtl numbers," *Physica D* **184**, 3–20.

Chandrasekhar, S., 1961, *Hydrodynamics and Hydromagnetic Stability*, Oxford University Press, Oxford.

Cross, M. C. and Hohenberg, P. C., 1993, "Pattern formation outside of equilibrium," *Revue of Modern Physics* **65**(3), 851–1112.

Eltayeb, I. A., 1972, "Hydromagnetic convection in a rapidly rotating fluid layer," *Proceedings of the Royal Society, London A* **326**, 229–254.

Eltayeb, I. A., 1975, "Overstable hydromagnetic convection in a rapidly rotating fluid layer," *Journal of Fluid Mechanics* **71**(1), 161–179.

Jaletzky, M. and Busse, F. H., 2000, "New patterns in centrifugally driven thermal convection," *Proceedings of the National Academy of Science* **97**, 5060–5064.

Kurt, E., Busse, F. H., and Pesch, W., 2004, "Hydromagnetic convection in a rotating annulus with an azimuthal magnetic field," *Theoretical and Computational Fluid Dynamics* **18**, 251–263.

Pesch, W., 1996, "Complex spatiotemporal convection patterns," *Chaos* **6**(3), 348–357.

Petry, M., Busse, F. H., and Finocchi, F., 1997, "Convection in a rotating cylindrical annulus in the presence of a magnetic field," *European Journal of Mechanics B/Fluids* **16**(6), 817–833.

Downloaded from http://jvc.sagepub.com at Gazi University on November 11, 2009